Erik P. Schartner, Georgios Tsiminis, Matthew R. Henderson, Stephen C. Warren-Smith, and Tanya M. Monro

Quantification of the fluorescence sensing performance of microstructured optical fibers compared to multi-mode fiber tips

Optics Express, 2016; 24(16):18541-18550

Published version http://dx.doi.org/10.1364/OE.24.018541

Research Article | Vol. 24, No. 16 | 8 Aug 2016 | OPTICS EXPRESS 18541

Optics EXPRESS

Quantification of the fluorescence sensing performance of microstructured optical fibers compared to multi-mode fiber tips

ERIK P. SCHARTNER,[1,2,*] GEORGIOS TSIMINIS,[1,2,3] MATTHEW R. HENDERSON,[1,2] STEPHEN C. WARREN-SMITH,[4] AND TANYA M. MONRO[1,2,5]

[1]*ARC Centre of Excellence for Nanoscale BioPhotonics, University of Adelaide, Adelaide, 5005, Australia*
[2]*Institute for Photonics and Advanced Sensing, School of Physical Sciences, University of Adelaide, Adelaide, 5005, Australia*
[3]*School of Medicine, The University of Adelaide, Adelaide, South Australia 5005, Australia*
[4]*Leibniz Institute of Photonic Technology (IPHT Jena), Albert-Einstein-Straße 9, 07745 Jena, Germany*
[5]*University of South Australia, Adelaide, Australia*
[*]*erik.schartner@adelaide.edu.au*

Abstract: Microstructured optical fibers, particularly those with a suspended-core geometry, have frequently been argued as efficient evanescent-field fluorescence-based sensors. However, to date there has not been a systematic comparison between such fibers and the more common geometry of a multi-mode fiber tip sensor. In this paper we make a direct comparison between these two fiber sensor geometries both theoretically and experimentally. Our results confirm that suspended-core fibers provide a significant advantage in terms of total collected fluorescence signal compared to multi-mode fibers using an equivalent experimental configuration.

OCIS codes: (060.2370) Fiber optics sensors; (060.4005) Microstructured fibers.

References and links

1. B. Lee, S. Roh, and J. Park, "Current status of micro-and nano-structured optical fiber sensors," Opt. Fiber Technol. **15**(3), 209–221 (2009).
2. X.-D. Wang and O. S. Wolfbeis, "Fiber-optic chemical sensors and biosensors (2013–2015)," Anal. Chem. **88**(1), 203–227 (2016).
3. X.-D. Wang and O. S. Wolfbeis, "Fiber-optic chemical sensors and biosensors (2008-2012)," Anal. Chem. **85**(2), 487–508 (2013).
4. T. M. Monro, S. Warren-Smith, E. P. Schartner, A. François, S. Heng, H. Ebendorff-Heidepriem, and S. Afshar, "Sensing with suspended-core optical fibers," Opt. Fiber Technol. **16**(6), 343–356 (2010).
5. M. E. Bosch, A. J. R. Sánchez, F. S. Rojas, and C. B. Ojeda, "Recent development in optical fiber biosensors," Sensors (Basel) **7**(6), 797–859 (2007).
6. E. P. Schartner, G. Tsiminis, A. François, R. Kostecki, S. C. Warren-Smith, L. V. Nguyen, S. Heng, T. Reynolds, E. Klantsataya, K. J. Rowland, A. D. Abell, H. Ebendorff-Heidepriem, and T. M. Monro, "Taming the light in microstructured optical fibers for sensing," Int. J. Appl. Glass Sci. **6**(3), 229–239 (2015).
7. S. C. Warren-Smith, S. Heng, H. Ebendorff-Heidepriem, A. D. Abell, and T. M. Monro, "Fluorescence-based aluminum ion sensing using a surface-functionalized microstructured optical fiber," Langmuir **27**(9), 5680–5685 (2011).
8. E. Schartner, M. Pietsch, A. Abell, and T. Monro, "A hydrogen peroxide fibre optic dip sensor for aqueous solutions," in *Australasian Conference on Optics, Lasers and Spectroscopy (2009: Adelaide, Australia)*, 2009.
9. P. Jorge, P. Caldas, C. Rosa, A. Oliva, and J. Santos, "Optical fiber probes for fluorescence based oxygen sensing," Sens. Actuators B Chem. **103**(1-2), 290–299 (2004).
10. F. Chu, G. Tsiminis, N. A. Spooner, and T. M. Monro, "Explosives detection by fluorescence quenching of conjugated polymers in suspended core optical fibers," Sensor. Actuat. Biol. Chem. **199**, 22–26 (2014).
11. J. B. Jensen, L. H. Pedersen, P. E. Hoiby, L. B. Nielsen, T. P. Hansen, J. R. Folkenberg, J. Riishede, D. Noordegraaf, K. Nielsen, A. Carlsen, and A. Bjarklev, "Photonic crystal fiber based evanescent-wave sensor for detection of biomolecules in aqueous solutions," Opt. Lett. **29**(17), 1974–1976 (2004).
12. E. Coscelli, M. Sozzi, F. Poli, D. Passaro, A. Cucinotta, S. Selleri, R. Corradini, and R. Marchelli, "Toward a highly specific DNA biosensor: Pna-modified suspended-core photonic crystal fibers," IEEE J. Sel. Top. Quantum Electron. **16**(4), 967–972 (2010).
13. S. C. Warren-Smith, G. Nie, E. P. Schartner, L. A. Salamonsen, and T. M. Monro, "Enzyme activity assays within microstructured optical fibers enabled by automated alignment," Biomed. Opt. Express **3**(12), 3304–3313 (2012).

#265314 http://dx.doi.org/10.1364/OE.24.018541
Journal © 2016 Received 16 May 2016; revised 14 Jul 2016; accepted 17 Jul 2016; published 3 Aug 2016

Optics EXPRESS

14. A. Leung, P. M. Shankar, and R. Mutharasan, "A review of fiber-optic biosensors," Sensor. Actuat. Biol. Chem. **125**, 688–703 (2007).
15. M. S. Purdey, J. G. Thompson, T. M. Monro, A. D. Abell, and E. P. Schartner, "A dual sensor for ph and hydrogen peroxide using polymer-coated optical fibre tips," Sensors (Basel) **15**(12), 31904–31913 (2015).
16. W. Henry, "Evanescent field devices: A comparison between tapered optical fibres and polished or d-fibres," Opt. Quantum Electron. **26**(3), S261–S272 (1994).
17. C. Bariain, I. R. Matías, F. J. Arregui, and M. Lopez-Amo, "Optical fiber humidity sensor based on a tapered fiber coated with agarose gel," Sensor. Actuat. Biol. Chem. **69**, 127–131 (2000).
18. L. C. Shriver-Lake, K. A. Breslin, P. T. Charles, D. W. Conrad, J. P. Golden, and F. S. Ligler, "Detection of tnt in water using an evanescent wave fiber-optic biosensor," Anal. Chem. **67**(14), 2431–2435 (1995).
19. C. M. Cordeiro, M. A. Franco, G. Chesini, E. C. Barretto, R. Lwin, C. H. Brito Cruz, and M. C. Large, "Microstructured-core optical fibre for evanescent sensing applications," Opt. Express **14**(26), 13056–13066 (2006).
20. S. Smolka, M. Barth, and O. Benson, "Highly efficient fluorescence sensing with hollow core photonic crystal fibers," Opt. Express **15**(20), 12783–12791 (2007).
21. E. P. Schartner, H. Ebendorff-Heidepriem, S. C. Warren-Smith, R. T. White, and T. M. Monro, "Driving down the detection limit in microstructured fiber-based chemical dip sensors," Sensors (Basel) **11**(12), 2961–2971 (2011).
22. E. P. Schartner, D. Jin, H. Ebendorff-Heidepriem, J. A. Piper, Z. Lu, and T. M. Monro, "Lanthanide upconversion within microstructured optical fibers: improved detection limits for sensing and the demonstration of a new tool for nanocrystal characterization," Nanoscale **4**(23), 7448–7451 (2012).
23. J. Zhao, D. Jin, E. P. Schartner, Y. Lu, Y. Liu, A. V. Zvyagin, L. Zhang, J. M. Dawes, P. Xi, J. A. Piper, E. M. Goldys, and T. M. Monro, "Single-nanocrystal sensitivity achieved by enhanced upconversion luminescence," Nat. Nanotechnol. **8**(10), 729–734 (2013).
24. S. Afshar V, Y. Ruan, S. C. Warren-Smith, and T. M. Monro, "Enhanced fluorescence sensing using microstructured optical fibers: a comparison of forward and backward collection modes," Opt. Lett. **33**(13), 1473–1475 (2008).
25. S. C. Warren-Smith, S. Afshar, and T. M. Monro, "Fluorescence-based sensing with optical nanowires: A generalized model and experimental validation," Opt. Express **18**(9), 9474–9485 (2010).
26. A. S. Webb, F. Poletti, D. J. Richardson, and J. K. Sahu, "Suspended-core holey fiber for evanescent-field sensing," Opt. Eng. **46**(1), 010503 (2007).
27. H. Ebendorff-Heidepriem, S. C. Warren-Smith, and T. M. Monro, "Suspended nanowires: fabrication, design and characterization of fibers with nanoscale cores," Opt. Express **17**(4), 2646–2657 (2009).
28. K. G. Casey and E. L. Quitevis, "Effect of solvent polarity on nonradiative processes in xanthene dyes: Rhodamine b in normal alcohols," J. Phys. Chem. **92**, 6590–6594 (1988).
29. J. Rheims, J. Köser, and T. Wriedt, "Refractive-index measurements in the near-ir using an abbe refractometer," Meas. Sci. Technol. **8**(6), 601–605 (1997).
30. S. Afshar V, S. C. Warren-Smith, and T. M. Monro, "Enhancement of fluorescence-based sensing using microstructured optical fibres," Opt. Express **15**(26), 17891–17901 (2007).
31. J. Arden, G. Deltau, V. Huth, U. Kringel, D. Peros, and K. H. Drexhage, "Fluorescence and lasing properties of rhodamine dyes," J. Lumin. **48**, 352–358 (1991).
32. B. Wajnchold, M. Grabka, A. Umińska, A. Ryguła, D. Kotas, M. Gołuński, S. Pustelny, and W. Gawlik, "Adsorption of cationic organic dyes in suspended-core fibers," Opt. Lett. **48-49**(8), 1647–1650 (2015).

1. Introduction

Optical fibers have been successful as optical sensing devices due to the combination of their small size, flexibility, low cost, and ability to measure in difficult to reach areas [1]. For the most part, optical fibers are used to deliver light to an area of interest and to collect the signal created locally as a result of the transduction mechanism. Amongst the different sensing modalities, fluorescence sensing has found many applications in chemical [2–4] and biological sensing [2,5,6] due to the large number of efficient fluorophores available and the strong optical signals they generate that make them ideal for optical sensing.

In optical fiber fluorescence sensing, a fluorophore, usually an organic dye, is introduced in the area of interest and is mixed with the sample. The optical fiber delivers excitation light, usually from a laser source, that is suitable to excite the fluorophore and generate fluorescence. The properties of this emission are determined by the fluorophore's interaction with the sample. The resulting fluorescence is collected by the optical fiber and is taken to a photodetector or spectrum analyzer for recording and analysis. Fiber-based fluorescence sensing has been deployed in sensing targets such as: aluminum ions [7], hydrogen peroxide [8], oxygen [9], and explosives [10]. Optical fiber based fluorescence sensors have also been deployed for biological applications, including measurements of biomolecules in solution [11], DNA [12], or enzyme assays within microstructured fibers [13].

Optics EXPRESS

The most established category of these sensors is based on multimode optical fibers (MMFs), where the sensing area is the cleaved tip of the fiber [14,15]. Fiber tip fluorescence sensing is simpler to deploy as the only part of the fiber that is exposed to the sample is the distal end, away from the excitation source, coupling optics and collection system. Tip sensing, however, can limit the amount of useful signal generated and collected as the sensing volume is limited to a small volume in close proximity to the optical fiber's tip.

Further work expanded on this concept to increase the interaction length, using methods such as removing side claddings to create D-fibers [16], or tapering [17,18] to spread the evanescent field outside of the glass core along the length of the fiber. Microstructured optical fibers have emerged in recent years as an alternative platform for optical fiber fluorescence sensing, as the internal structure of those fibers can result in greatly increased interaction area between the light and the sample [4,19–21]. Suspended core microstructured optical fibers (SCFs) in particular, having a small strut-suspended glass core surrounded by a number of voids along the entire length of the fiber, enable a fraction of the optical field to extend evanescently into the voids where it interacts with the analyte along the length of the fiber [4]. These fibers require minute sample quantities, in the order of a few nanoliters, and have been successfully deployed in fluorescence sensing with sensitivities as low as single particle detection [22,23].

An interesting question when considering which of the two optical fiber platforms to use for a particular sensing application is which of them gives a higher signal, and therefore lower detection limits for a given excitation power and fluorophore concentration. While comparison has previously been made between D-shaped and tapered fibers [16], to date a comparison between SCFs and tip fibers has not been covered. Previous work has examined the fluorescence capture into the guided modes of these SCFs [24], and then verified these theoretical results against experimental data [25]. In this study we seek to extend this to give a direct comparison of expected fluorescence intensities in comparable conditions.

The long interaction length between the guided optical modes and the analyte in SCFs is counteracted by the low intensity of the part of the guided field inside the void compared to the peak intensity at the center of the glass core [4,26]. In contrast, the MMFs have the opposite set of features, with high intensities available at the tip but over a very limited area. Further to those considerations, the amount of fluorescence generated and captured per unit excitation power and area of fiber means that deciding between the two platforms becomes a more complicated process.

In this work we present a direct experimental comparison between MMF tip sensors and SCF sensors for fluorescence sensing. We show that SCFs collect a higher fluorescence power per unit of input power and therefore have a potential detection limit advantage over MMFs.

2. Experimental method

2.1 Sample preparation

Rhodamine B (Sigma-Aldrich, USA) was diluted to a concentration of 1 mM in ethanol. Serial dilutions were then prepared to give a range of concentrations for measurements, and pipetted to individual containers for experiments to minimize potential effects of evaporation.

2.2 Multi-mode fibers

Two commercial multi-mode fibers were used, with core diameters of 62.5 μm (Corning Multimode 0.275 NA) and 105 μm (Thorlabs FG105UCA 0.22 NA).

The experimental configuration for fluorescence measurements is shown in Fig. 1. A 532 nm laser source (Laser Quantum Gem) was passed through a set of neutral density (ND) filters to vary the transmitted power. A mechanical shutter was used to block excitation light outside of fluorescence collection windows. Incident pump light was then reflected off a near-normal incidence 532 nm long pass (LP) filter (Semrock Razoredge Ultrasteep). A 10 × 0.25

Optics EXPRESS

numerical aperture (NA) microscope objective was used to couple the light into the multi-mode fibers, and the coupling maximized by monitoring the transmitted power.

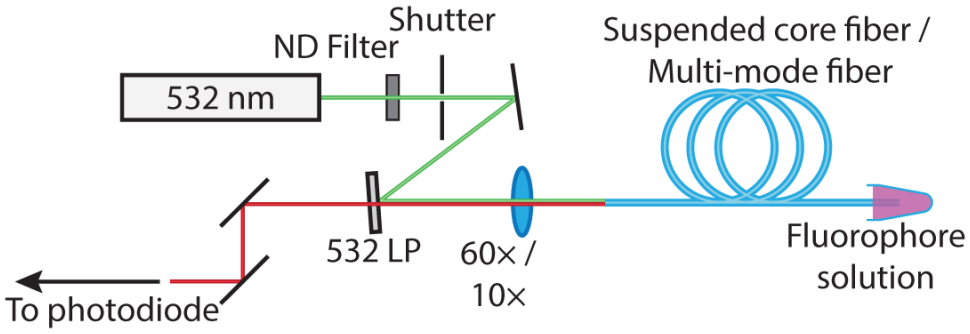

Fig. 1. Experimental configuration for measurements of emitted fluorescence power for both multi-mode (10x microscope objective) and SCFs (60x microscope objective). A calibrated photodiode was used as the detector for these trials.

The combined optical loss through each element was recorded prior to measurements using a calibrated photodiode. This allowed for the measurement of the fluorescence power at the end face of the optical fiber to be inferred from the measurement of the power at the distal end of the coupling fiber in the diagram above. Background fluorescence and residual pump light levels were recorded by immersing the fiber tip in ethanol, and recording the measured power across a range of excitation powers. This background value was then subtracted from the overall signal value to give the contribution of the power arising from the fluorophore alone.

Measurements were performed by immersing the tip of the fiber in the fluorophore solution and recording the measured fluorescence power over a range of excitation powers. The fiber tip was maintained at a fixed distance (10 mm) from the bottom of the sample vial, and measurements performed across multiple vials to ensure sample consistency and reproducibility of measured power values. This distance was chosen as the theory (see Sec. 3.1) has shown a limited contribution in the fluorescence collected from distances over 4 mm away from the tip of the fiber. The fluorescence power at the end face of the optical fiber was then inferred from the measurement of the power at the specified location in the diagram above using the correction factor recorded earlier. The collection fiber was then replaced and the next fluorophore concentration measured.

2.3 Suspended core fibers

SCFs were fabricated from F300HQ Suprasil (Heraeus Quartzglass) using a two-step drawing process similar to that described in [13]. The initial preform was fabricated by ultrasonic drilling, before being caned and inserted into a jacket before being drawn to fiber. The final fiber core size (effective core diameter [27]) was measured using a scanning electron microscope (SEM) as 1.38 µm, while the surrounding voids had a diameter of 15 µm. The fiber geometry is shown in Fig. 2 below. For fluorescence sensing experiments a 25 cm length of fiber was used.

Optics EXPRESS

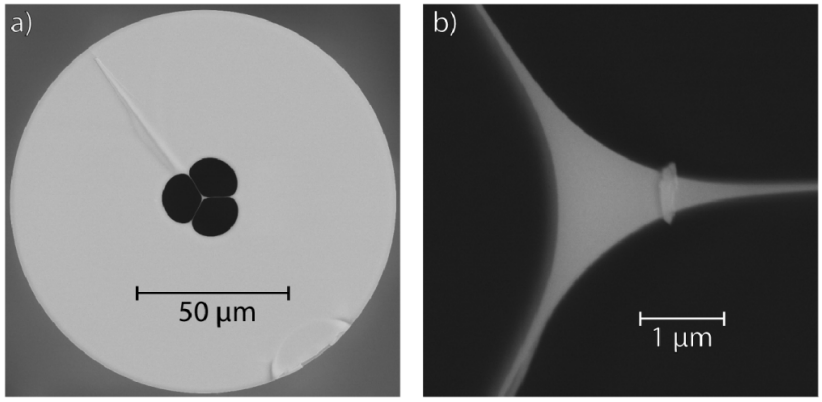

Fig. 2. Silica SCFs used for fluorescence experiments. (a) Full geometry, 125 µm outer diameter with 15 µm holes. (b) Core structure, with a core diameter of 1.38 µm.

Fluorescence measurements were performed using a similar method to that described earlier, using the experimental configuration shown in Fig. 1. A 60x microscope objective was used for coupling excitation light into the core of the fiber, and coupling was optimized by monitoring the transmitted power using a calibrated photodiode. The fiber was filled by immersing the distal tip of the fiber into the fluorophore solution for a period of five minutes, which was sufficient to fill 20 cm of the total 25 cm length of fiber. Once the given time had elapsed the tip of the fiber was removed from the solution and measurements performed at different levels of input power. The observed fluorescence signal was recorded for each input power, and the previous optical loss information used to convert the measured value to the actual fluorescence power captured within the fiber.

3. Experimental results and theoretical analysis

3.1 Multimode fiber tip sensors

The collection efficiency of the 62.5 µm and 105 µm core MMFs fibers was theoretically simulated by examining the portion of light recaptured into the collection cone from emitters located beyond the tip of the fiber. The collection efficiency across the emission wavelength range was calculated and the results integrated to give the total fluorescence power emitted from the fluorophores. Literature values of absorption and emission coefficients for rhodamine B in ethanol [28] were used for the entirety of both the multi-mode and suspended core theoretical calculations.

The collected power was calculated by a ray trace calculation, as the fiber core was large enough to assume ray optics. The fiber was modelled with an acceptance angle based on the fiber NA, such that any ray that is incident on the fiber core at an angle equal to or less than the acceptance angle would be counted as guided by the fiber and so add to the total power captured. A schematic of the model is shown in Fig. 3. The output of the pump light was taken to be a cone with angle based on the NA of the fiber. Output and acceptance angles were also adjusted based on the refractive index of the fluorophore solution at the respective wavelengths, with the index calculated via a dispersion equation for ethanol [29].

Optics EXPRESS

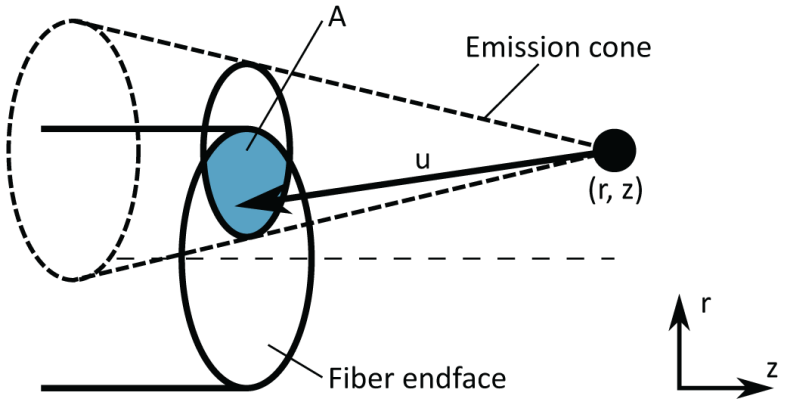

Fig. 3. Schematic of the theoretical power capture into the collection cone of an emitter located a fixed distance away from the tip of a MMF

The pump light cone region was discretized spatially into a grid of points radially (r) and longitudinally along the direction of the fiber (z). Captured power into the fiber was calculated for each point and then integrated over r and z. The ray trace equations are independent of azimuthal angle θ due to rotational symmetry about the fiber axis, giving a constant 2π factor for the final integration over theta.

The fraction of captured power from each (r, z) point was calculated by evaluating the solid angle subtended by the fiber endface at that point and dividing by total solid angle 4π. The solid angle integral included an absorption factor to account for fluorophore reabsorption. Guided rays were selected by only considering rays emitted by the (r, z) point in a cone with half-angle equal to the fiber acceptance angle, as these are the only rays able to be guided within the fiber. The solid angle calculation was thus over an area formed by the intersection of this emission cone with the fiber endface. The equation for the captured power fraction (CF) is given by Eq. (1).

$$CF = \frac{1}{4\pi}\iint_A e^{-|\mathbf{u}|\alpha}\frac{z}{|\mathbf{u}|^{3/2}}dA \tag{1}$$

where $|\mathbf{u}|$ is the vector from the (r, z) point to an infinitesimal area dA and α is the absorption coefficient. The solid angle was calculated by discretizing the intersection area into a grid of points and evaluating the integral using trapezoidal integration. The intersection area is calculated as the intersection of two circles, where one is the fiber endface and the other is the slice of the 'emission cone' at the z of the fiber endface.

Each point was multiplied by the absorbed power to account for pump power absorption. Absorbed power was calculated for each z-slice using Beer's law. The entire calculation was repeated over the fluorophore emission spectrum, sampling the reabsorption at each fluorophore emission wavelength. The results of this were then multiplied by the normalized fluorescence emission spectra to obtain the total power captured by the fiber. Model parameters, such as number of grid points and ray angles, were convergence tested. No free parameters were used for fitting.

The collection efficiency was calculated for a range of concentrations, and scaled for the input power used in the experimental measurements described above. The results of the experimental trials, Sec. 2.1, and the theoretical analysis are shown in Fig. 4 below. The model presented here approximates the collection into the 62.5 μm graded index fiber as a step-index fiber with the same core size and numerical aperture.

Optics EXPRESS

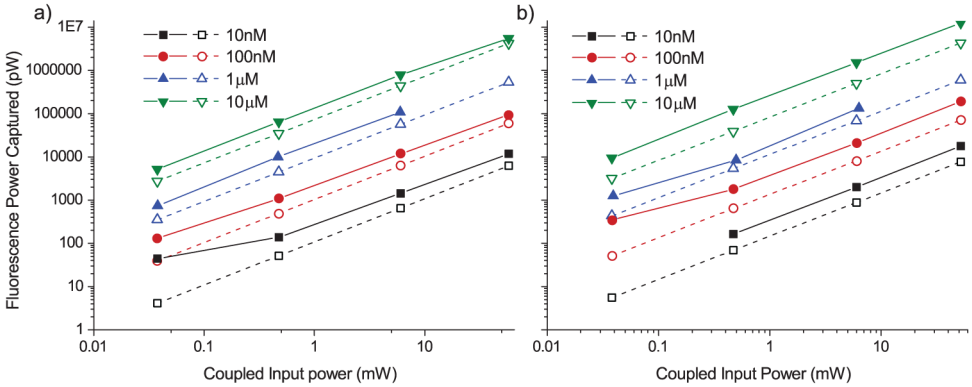

Fig. 4. Fluorescence Capture for MMFs, showing comparison between experimental (filled symbols) and theoretical (open symbols) for (a) 62.5μm core diameter (NA = 0.275) MMFs and (b) 105 μm core diameter (NA = 0.22) MMFs.

These results show a strong correlation between the measured experimental fluorescence power and the corresponding calculated theoretical power, though with the experimental power consistently slightly higher than the theoretical values. As expected, a higher signal is naturally observed for the larger 105 μm core fiber, Fig. 4(b), than is seen from the 62.5 μm fiber, Fig. 4(a), with a maximum increase of 1.8 × in the collected signal. This difference can be explained primarily from the area of the fiber tips (8660 μm^2 c.f. 3067 μm^2 for 105 μm and 62.5 μm, respectively), as well as the difference in NA between the two fibers (0.22 cf. 0.275).

For most experimental conditions tested there is a linear increase in fluorescence with increasing input power. Some deviation is seen between measurements at the lowest excitation powers (33/38 μW) for low fluorophore concentrations as the fluorescence signal intensity becomes comparable to the background signal from the ethanol, increasing the relative error of the measurements. Also, at low concentrations the signal from the fluorophore is lower than the background signal from unfiltered pump light, or autofluorescence from the glass itself [21].

3.2 Suspended core fiber sensors

A full vectorial model to simulate the captured fluorescence was used, based on a model previously presented in [25, 30]. This model is based on a step-index glass-ethanol geometry, which is a close approximation to the suspended-core fiber geometry.

This model was modified to consider a range of emission wavelengths covering the emission band of rhodamine B in ethanol [31], again applying the dispersion equation utilized in the tip collection calculations in Sec. 3.1. The calculated emission was then normalized to the literature emission spectra of rhodamine B and summed to give the total overall fluorescence capture.

For the core size used in this work (core diameter 1.38 μm) the experimentally measured fluorescence power was compared against the results expected by the modeling and are plotted together in Fig. 5.

Optics EXPRESS

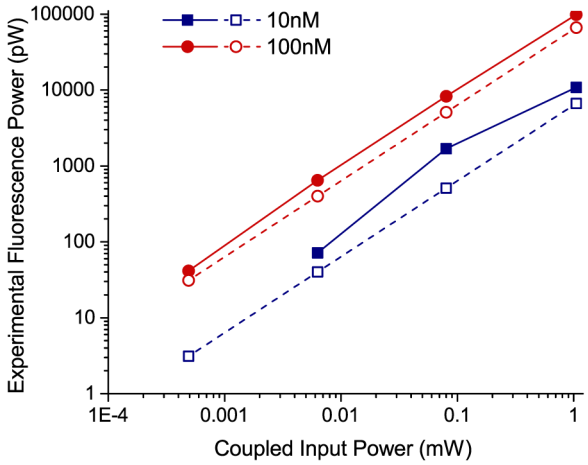

Fig. 5. Fluorescence power captured for suspended core optical fibers, showing comparison between experimental (filled symbols) and theoretical (open symbols) across the full range of excitation powers used.

The measured values are in good agreement with the numerical calculations across a range of concentrations and excitation powers, with the experimental results consistently showing a slightly higher result than the theoretical prediction. This could be due to variations in the coupled modes, adsorption of cationic dye onto the negatively charged silica glass [32] acting to increase the local fluorophore concentration on the surface, or the use of a step-index approximation.

3.3 Comparison between suspended-core and multi-mode fibers

In Fig. 6 the data from Figs. 4 and 5 is combined in order to give a comparison between the suspended-core and multi-mode fibers for a given coupled input power level for a fixed fluorophore concentration (100 nM).

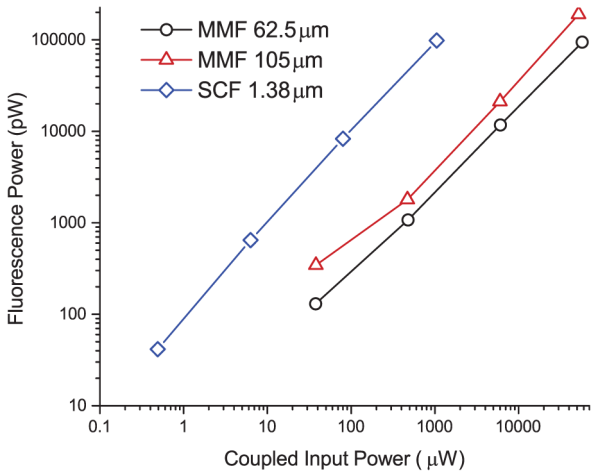

Fig. 6. Comparison of experimentally measured fluorescence between suspended core and multi-mode fibers.

Based on the linear dependence of fluorescence power versus fiber coupled power shown in Fig. 6, a good way to compare the performance of these fiber sensors is to examine their sensing efficiency, defined as the total fluorescence power collected divided by the coupled excitation power. Furthermore, since at low fluorophore concentrations changes in

Optics EXPRESS

concentration have minimal effect on the linear relationship between fluorescence power and coupled power, we can use efficiency per concentration (in μM) as a way of comparing the two different optical fiber sensing platforms. For the particular case study in this work the SCF sensors have an efficiency of 9.7×10^{-4} μM^{-1}, whereas the 105 μm MMF tip sensors show an efficiency of 1.8×10^{-5} μM^{-1}. These results show that for fibers and lengths used here the SCF s show an efficiency that is 55 × higher than the MMFs.

Previous work [25] has verified the performance of the theoretical model across a range of core sizes for the SCFs. Our current model for the MMF tip sensors can also predict the influence of a changing tip diameter on the NA and fluorescence collection efficiency. A comparison of the predicted total fluorescence power captured by different core (SCFs) and tip (MMFs) diameters is shown in Fig. 7 below for 1 mW input power, with a 10 nM rhodamine B concentration.

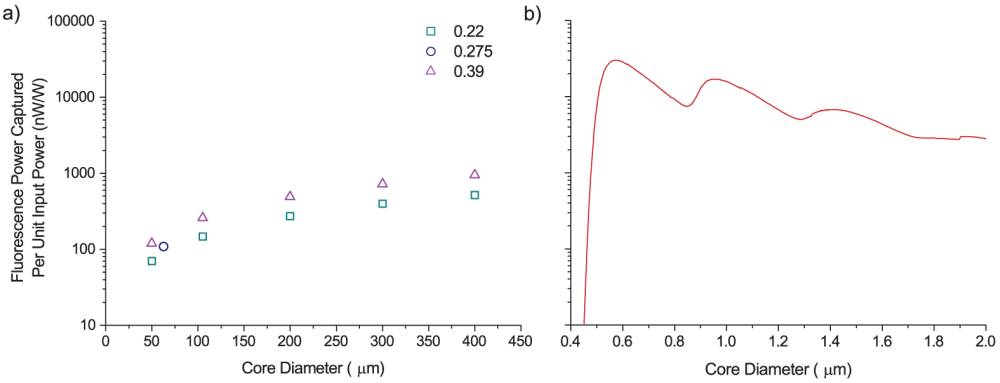

Fig. 7. Fluorescence power captured per unit input power for 10 nM Rhodamine B in ethanol (a) Multi-mode tip sensors for step index fibers of varied diameters (0.22,0.39) and graded-index (0.275) (b) Silica SCF

These results show that, for a given excitation power and fluorophore concentration, SCFs show a consistently higher signal than MMFs at all practical core sizes. Even considering the largest readily available high NA fiber from www.thorlabs.com, with a 1 mm core size and 0.5 NA the fluorescence capture model shows a power capture of 2850 nW/W, which is significantly lower than the 1.38 μm core size fiber used in the experimental trials here (6660 nW/W), and comparable to the result obtained from the largest SCF core size fibers modeled here (2790 nW/W at 2 μm core diameter). It is also interesting to compare the effect of total sensing area on the performance of these fiber sensors. For the MMF tip sensors, the sensing area is the tip of the fiber, measuring 3068 μm^2 for the 62.5 μm and 8660 μm^2 for the 105 μm fiber. For the SCF sensors, the sensing area is the area of the 20 cm long segment of the core surrounded by the liquid sample, measuring approximately 867,000 μm^2, 282 × and 100 × the tip area of the 62.5 μm and 105 μm fibers respectively. This shows that although the collection efficiency of the SCFs is lower than the MMFs, this is compensated for by the significantly enhanced surface area of the SCFs leading to a significantly higher fluorescence signal across the explored range.

For low concentrations additional significant improvements to the performance of the SCFs can be obtained by increasing the length of the fibers, however this comes at the cost of the total measurement time due to the need to fill a greater length of SCF for filling or the increased experimental complexity of including a flow-cell or pressure filling arrangement to increase filling speeds.

4. Conclusion

We have investigated the performance of two different types of optical fiber fluorescence sensor, namely the established multimode optical fiber (MMF) tip sensors and the suspended core optical fiber (SCF) sensors. Theoretical modeling for both types of fiber sensors is in

Optics EXPRESS

good agreement with experimental measurements on the total fluorescence power captured by each sensor as a function of dye concentration in the sample and excitation power.

The results shown here are also applicable to alternate sensing geometries such as tapered fibers or nanowires, where the fluorescence is also integrated along the length. In the future, multi-core fibers could also be considered for the end-face collection, by examining the collection into the individual cores and accounting for the excitation/collection coupling efficiency at the opposite end of the fiber. These results should also be readily transferable to other fluorophores with isotropic light emission, as long as the quantum efficiency and absorption coefficient are known and the experimental conditions minimize absorption saturation and fluorescence quenching.

Experimental results show that for the particular parameters studied here, which are based on practical considerations, SCF fluorescence sensors are up to 55x more efficient in comparison to MMF tip sensors, highlighting their excellent potential as low detection limit fluorescence sensors. Further theoretical analysis has demonstrated that SCFs have an improved sensitivity compared to MMFs across a large parameter space, showing that the use of these fibers is advantageous in optical fiber fluorescence sensing applications where low detection limits are required.

Funding

Australian Research Council (ARC) (CE140100003, LP110200736, FL130100044), National Breast Cancer Foundation (Australia, NBCF) (NC-13-05), European Commission (PIIF-GA-2013-623248)

Acknowledgments

The authors would like to acknowledge the assistance of Mr Peter Henry and Mr Alastair Dowler in fabrication of the suspended core optical fibers, and Dr Malcolm Purdy for fruitful discussions. This work was performed in part at the OptoFab node of the Australian National Fabrication Facility.